J. Fluid Mech. (1980), *vol.* 97, *part* 2, *pp.* 279–297
Printed in Great Britain

Buoyancy force reversals in vertical natural convection flows in cold water

By VAN P. CAREY, BENJAMIN GEBHART AND JOSEPH C. MOLLENDORF

Department of Mechanical Engineering, State University of New York at Buffalo, Amherst, New York 14260

(Received 15 February 1979 and in revised form 1 May 1979)

Calculated numerical results are presented for laminar buoyancy-induced flows driven by thermal transport to or from a vertical isothermal surface in cold pure and saline water wherein a density extremum arises. The present calculations specifically explore the consequences of temperature conditions wherein the buoyancy force reverses across the thermal region owing to the presence of a density extremum within the region. Such conditions commonly occur in terrestrial waters and in technological processes utilizing cold water. The linear approximation of density dependence on temperature, used in conventional analysis, is here replaced by a very accurate non-linear density equation of state for both pure and saline water. This permits an accurate treatment of such flows for bounding temperatures up to 20 °C at ambient salinity and pressure levels from 0 to 40 p.p.t. and 1 to 1000 bars, respectively. The results may be applied to the melting or slow freezing of a vertical ice surface in pure water as well as to a heated or cooled vertical isothermal surface in pure or saline water. For example, buoyancy force reversals arise for a vertical ice surface at 0 °C melting in fresh water between 4 °C and 8 °C at atmospheric pressure. Temperature conditions for which buoyancy force reversals occur are of special interest because of the resulting anomalous flow behaviour and low surface heat-transfer rates. The transition from conditions with no buoyancy-force reversal to those resulting in a large buoyancy-force reversal is accompanied by as much as 50 % decrease in surface heat transfer. This produces a corresponding trend in the melt rate of a vertical ice surface in pure water. Sufficiently strong buoyancy force reversals are found to cause local flow reversal either at the edge of the flow layer or near the surface. Conditions are determined for which flow reversals occur at each of these locations. These local flow reversals are the precursors of convective inversion, that is, of the reversal of the net flow direction with changing ambient medium temperature. Limits on conditions for convective inversion are determined. Calculated transport is compared with previous experimental results, with good agreement throughout the several regions of such complicated flows. The calculations indicate that such flows are relatively very weak. However, their form may lead to early laminar instability.

0022–1120/80/4405–8500 $02.00

1. Introduction

Buoyancy-induced flows in cold pure and saline water are a very common occurrence in our environment and in many processes in technology. The mechanisms of such flows are often considerably complicated by the occurrence of a density extremum with temperature variation. Consider, for example, a surface at a temperature of 8 °C in ambient pure water at 1 bar pressure and at a uniform temperature of 2 °C. Near the surface, the fluid is less dense than the ambient and the buoyancy force is upward. However, since the extremum for pure water at 1 bar occurs at about 4 °C, the fluid in the outermost portion of the thermal-transport region is more dense than the ambient. The buoyancy force there is downward. Hence, this pair of bounding temperatures results in buoyancy-force reversal across the thermal-diffusion region. Such temperature conditions are very common. In addition, these kinds of complications are also found in cold water to high pressure and even at moderate salinity. The extremum persists, before an equilibrium-phase interface, to a pressure of about 300 bars. In saline water at 1 bar, it is still found to a salinity s of about 26‰ (p.p.t.). Even beyond these limits, the density variation of water, in tending toward an extremum, remains strongly nonlinear.

As a consequence, a linear approximation of the temperature effect on density may not be used to estimate the motion-driving buoyancy force $F = g(\rho_r - \rho)$, where ρ_r and ρ are a reference density and the local density in, for example, a thermal transport region in the fluid.

Gebhart & Mollendorf (1978) summarize earlier studies of such convective motions and give a comprehensive method of analysing such flows in thermally-buoyant pure and saline water. The formulation and results apply to a flow generated adjacent to a vertical surface at temperature t_0, in a quiescent ambient medium at t_∞. These results are compared with data from the ice-melting experiments of Bendell & Gebhart (1976), with close agreement.

In more recent studies, other vertical laminar boundary-layer flows in pure and saline water have been analysed in the manner of Gebhart & Mollendorf (1978). Qureshi & Gebhart (1978) have computed similarity solutions for the flow adjacent to a vertical uniform-heat-flux surface in ambient water at t_m, the temperature corresponding to maximum density. The axisymmetric and plane plume flows in water at t_m have been analysed by Mollendorf, Johnson & Gebhart (1980). The perturbation analysis of Gebhart, Carey & Mollendorf (1980) extends the results of Qureshi & Gebhart (1978) and Mollendorf, Johnson & Gebhart (1980) to ambient water temperatures not equal to t_m.

The bases of these analyses are two. The first is a new state equation for the density of pure and saline water, developed by Gebhart & Mollendorf (1977), which is very accurate and quite simple for convective analysis. It contains only one temperature term. It is an expansion of density $\rho(t, s, p)$ around the temperature at which the extremum occurs, $t_m(s, p)$, at given salinity and pressure levels, s and p. The equation was developed as a fit of the most modern density information, the correlation of Fine & Millero (1973) for pure water and the data of Chen & Millero (1976) for saline water. In the range of conditions from 0 to 20 °C, to 1000 bars, the r.m.s. fit for pure water is to 3·5 p.p.m. For saline water, for the same t and p ranges, the r.m.s. fit is 10·4 p.p.m., to a salinity of 40‰. Recall that oceanic salinity is about 35‰. Thus the equation encom-

passes a preponderant fraction of all terrestrial surface waters. The form of the equation is

$$\rho(t,s,p) = \rho_m(s,p)\,[1-\alpha(s,p)\,|t-t_m(s,p)\,|^{q(s,p)}] \tag{1}$$

where $\rho_m(s,p)$, $\alpha(s,p)$, $t_m(s,p)$ and $q(s,p)$ were determined to give the best fit, in the r.m.s. sense, to the density information. The functional forms and evaluation of these four quantities are given in detail by Gebhart & Mollendorf (1977, 1978).

The second aspect of the treatment for thermally buoyant flows is the transformation of the boundary region flow equations to equations in terms of similarity variables. The present study considers the laminar buoyancy-induced flow adjacent to a heated or cooled vertical isothermal surface in cold water. The compact formulation used here is that of Gebhart & Mollendorf (1978). Salinity and static pressure are assumed constant throughout the flow. Gebhart & Mollendorf (1978) have shown that, for the isothermal surface condition, this formulation yields similarity solutions. These depend only on $q(s,p)$, the Prandtl number Pr, and $R = (t_m(s,p)-t_\infty)/(t_0-t_\infty)$. The formulation therefore applies to flow adjacent to a heated or cooled isothermal surface for any temperature, salinity and pressure conditions within the range of validity of the density correlation. It may also be applied to the melting or slow freezing of a vertical ice surface in pure water ($s = 0$). For ice melting or freezing in saline water, salinity buoyancy and diffusion effects must be taken into account. Such effects are not included here. The present analysis applies only to flows driven by thermal buoyancy in cold pure or saline water. It does not apply to ice melting or freezing in saline water.

Over the range of bounding temperatures considered here, the buoyancy force will be bi-directional across the thermal layer. The buoyancy force will act in the upward direction near the surface, while in the outer portion of the thermal layer it will act downward. The variation of the buoyancy force across the thermal boundary-layer depends primarily on the relation of the values of the surface temperature, t_0, and the ambient temperature, t_∞, to $t_m(s,p)$. The results of Gebhart & Mollendorf (1978) indicate that for $R = (t_m-t_\infty)/(t_0-t_\infty) \leqslant 0$, the buoyancy force and flow are upward. For $R \geqslant 0{\cdot}5$, they are both downward.

Gebhart & Mollendorf (1978) have computed numerical results for a wide range of R outside the interval $0 < R < 0{\cdot}5$, for various values of Prandtl number and $q(s,p)$. However, numerical solutions were not obtained for R between 0 and $\frac{1}{2}$. For all such flows the buoyancy force is bi-directional across the thermal layer. The most complicated flow and thermal transport characteristics occur in this range. Convective inversion is defined as reversal of the direction of net mass flow with changing R. Clearly, for flows in pure and saline water driven by thermal buoyancy alone, convective inversion must occur at some value of R between 0 and $\frac{1}{2}$. The experiments of Bendell & Gebhart (1976) indicate that this occurs at about $R = 0{\cdot}28$ for ice melting in pure water.

As will later be seen, the approach to convective inversion from both $R = 0$ and $R = \frac{1}{2}$ is characterized by a rapid decrease in flow vigour and surface heat transfer. For conditions very near convective inversion, the tangential velocity is bi-directional, up near the surface and down in the outer portion of the flow region. As convective inversion is approached, bi-directional flow first appears as small local flow reversals. These occur near the surface for R decreasing from $\frac{1}{2}$ and near the outer edge of the flow

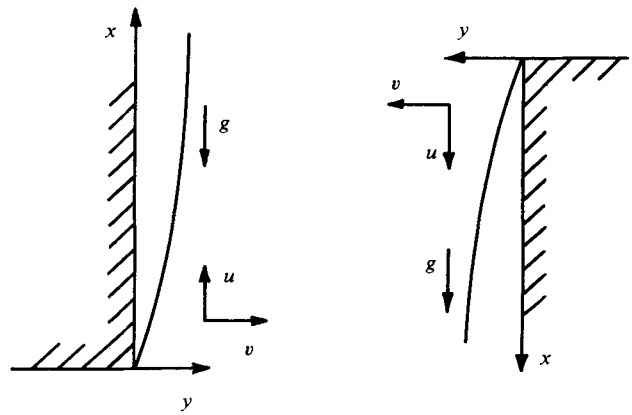

(a) (b)

FIGURE 1. Co-ordinate systems for the two flow regimes: (a) net upward flow, for R near 0, and (b) net downward flow, for R near $\frac{1}{2}$.

region for R increasing from 0. Such consequences were not evaluated in any detail by Gebhart & Mollendorf (1978) owing to insurmountable difficulties in the numerical scheme used. However, the experiments of Bendell & Gebhart (1976) and of Johnson & Mollendorf (1980) include many flows for which R lies between 0 and $\frac{1}{2}$.

The numerical treatment employed here has overcome many of these difficulties. Boundary-layer similarity solutions are presented across most of the range of R between 0 and $\frac{1}{2}$. Calculated thermal transport is compared with the experimental results of Bendell & Gebhart (1976) and of Johnson & Mollendorf (1980). The values of R which first result in local flow reversal are determined for reversal near the surface and near the outer edge of the flow. Limits are also obtained on the conditions for convective inversion.

2. Analysis

For R between 0 and $\frac{1}{2}$, with a local buoyancy-force reversal across the thermal region, two distinct flow regimes arise. The first is net upflow, figure 1 (a), with x positive in the upward direction and g acting in the negative x direction. The second flow regime, in figure 1 (b), is net downward flow, with x positive in the downward direction and g acting in the positive x direction. Flows with values of R near 0 correspond to the first regime and those near $\frac{1}{2}$ correspond to the latter. For values of R near the centre of the interval, $0 \leqslant R \leqslant \frac{1}{2}$, it is not apparent, *a priori*, which net flow direction results and which co-ordinate system applies. At the outset, it is postulated that the choice of co-ordinate system be dictated by the direction of net mass flow in the convection region. This assumption will later be examined in light of the calculated results. For the two co-ordinate systems, the net mass flow is in the positive x direction, but the sign of g is different. We will, therefore, adopt a '$\pm$' sign on g, where '+' corresponds to net downflow and '$-$' corresponds to net upflow.

The resulting laminar boundary-layer equations are written below. As indicated in figure 1, x is the distance downstream from the leading edge along the surface, and

y is normal thereto. The velocities $u(x, y)$ and $v(x, y)$ are the tangential (x) and normal (y) components, and $t(x, y)$ is the local temperature:

$$\frac{\partial u}{\partial x}+\frac{\partial v}{\partial y}=0, \tag{2a}$$

$$u\frac{\partial u}{\partial x}+v\frac{\partial u}{\partial y}=\nu\frac{\partial^2 u}{\partial y^2}\pm g(\rho_\infty-\rho)/\rho_r, \tag{2b}$$

$$u\frac{\partial t}{\partial x}+v\frac{\partial t}{\partial y}=\alpha\frac{\partial^2 t}{\partial y^2}; \tag{2c}$$

$$u(x,0)=v(x,0)=u(x,\infty)=0, \quad t(x,0)=t_0 \quad \text{and} \quad t(x,\infty)=t_\infty. \tag{3}$$

In equations (2b) and (2c) $F=\pm g(\rho_\infty-\rho)/\rho_r$ is the local buoyancy force per unit volume and ν and α are the kinematic viscosity and thermal diffusivity of the fluid, respectively.

The buoyancy force in (2b) is evaluated from (1). Then (2) and (3) are transformed in terms of a similarity space co-ordinate, η, a stream function $\psi(x, y)$ or $f(\eta, x)$ and temperature function $\phi(\eta, x)$, as follows:

$$\rho_\infty-\rho=\rho_m(s_\infty,p)\,\alpha(s_\infty,p)\,[|\phi-R|^{q(s_\infty,p)}-|R|^{q(s_\infty,p)}]=\rho_m\alpha W; \tag{4}$$

$$R=\frac{t_m(s_\infty,p)-t_\infty}{t_0-t_\infty}=R(s_\infty,p,t_0,t_\infty); \tag{5}$$

$$\eta=yb(x), \quad \psi=\nu c(x)f(\eta), \tag{6a}$$

$$t_0-t_\infty=d(x), \quad \phi=(t-t_\infty)/(t_0-t_\infty), \tag{6b}$$

$$c(x)=4(Gr_x/4)^{\frac{1}{4}}=G, \quad b=G/4x; \tag{6c}$$

$$Gr_x=\frac{gx^3}{\nu^2}\alpha(s_\infty,p)|t_0-t_\infty|^q; \tag{7}$$

$$f'''+3ff''-2f'^2\pm[|\phi-R|^q-|R|^q]=0, \tag{8a}$$

$$\phi''+3Prf\phi'=0, \tag{8b}$$

$$f(0)=f'(0)=f'(\infty)=1-\phi(0)=\phi(\infty)=0. \tag{8c}$$

Similarity is seen in (8) to result for both R and $q(s_\infty, p)$ constant for an unstratified ambient, i.e. constant t_∞. Then f and ϕ depend only on η. The parameters then are R and $q(s_\infty, p)$, in addition to the Prandtl number Pr. Note above that Gr_x is here differently defined than that by Gebhart & Mollendorf (1978). Here, the units of buoyancy are taken as $\alpha|t_0-t_\infty|^q$ rather than as $\alpha|t_0-t_\infty|^q I_w$, where

$$I_w=\int_0^\infty W\,d\eta. \tag{9}$$

In that formulation W becomes W/I_w in (8a). Here, I_w does not appear in (8a) and it is therefore not necessary to iteratively determine I_w when solving the equations. The variables of Gebhart & Mollendorf (1978), GM, are related to the present ones as follows:

$$\eta=\eta_{\rm GM}\,|I_w|^{-\frac{1}{4}}_{\rm GM}, \tag{10a}$$

$$\phi'=\phi'_{\rm GM}\,|I_w|^{\frac{1}{4}}_{\rm GM}, \tag{10b}$$

$$f=f_{\rm GM}\,|I_w|^{\frac{1}{4}}_{\rm GM}, \quad f'=f'_{\rm GM}\,|I_w|^{\frac{1}{2}}_{\rm GM}, \tag{10c}$$

$$f''=f''_{\rm GM}\,|I_w|^{\frac{3}{4}}_{\rm GM}, \quad I_w=(I_w)_{\rm GM}\,|I_w|^{-\frac{1}{4}}_{\rm GM}. \tag{10d}$$

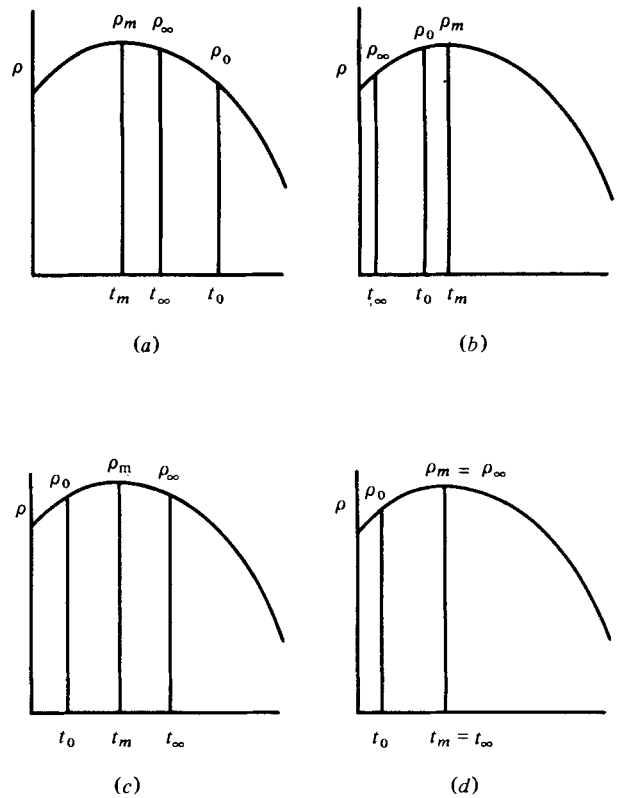

FIGURE 2. The effect of the specified conditions t_0 and t_∞ on $R = (t_m - t_\infty)/(t_0 - t_\infty)$, on the buoyancy force, F, and on flow direction. (*a*) $F > 0$, $R < 0$ and flow is up; (*b*) $F < 0$, $R > 0$ and flow is down; (*c*) $F \leqslant 0$, $R = \frac{1}{2}$ and flow is down; (*d*) $F > 0$, $R = 0$ and flow is up.

The role of R is crucial in the formulation given in (4)–(8) above. It is the quantitative expression of the effect of the extremum behaviour on the resulting flow characteristics. It places the specific temperature conditions, t_0 and t_∞, with respect to $t_m(s, p)$. Specifically, the value of R indicates the nature of the local variation and the direction of the buoyancy force F. In figure 2 several characteristic choices of t_0 and t_∞ are shown on a plot of $\rho(t, s, p)$ versus t for given values of s and p. For figure 2(*a*, *b*), where $t_0 > t_\infty$, $F > 0$ and $F < 0$, respectively, across the whole thermal diffusion region. Flow is up for (*a*) and down for (*b*). Note that $R_a < 0$ and $R_b > 0$. For t_0 taken less than t_∞, relations reverse. For figure 2(*c*), $R = \frac{1}{2}$ and $F < 0$, except at the fluid–surface interface where $F = 0$; flow is down.

However, a decrease of t_0, $R < \frac{1}{2}$, will in fact cause a region of buoyancy-force reversal ($F > 0$) adjacent to the surface. This may lead to an upward local flow reversal there. For figure 2(*d*), $R = 0$ and $F > 0$, and flow is upward. However, if t_∞ is increased from t_m, $R > 0$. Then F becomes negative in the outer part of the thermal region and a downward local flow reversal could occur there.

Thus, in coming into the region $0 < R < \frac{1}{2}$ from each side, local buoyancy-force reversals arise. These may lead to local flow reversals. The net flow is down when coming in from the upper R limit, $\frac{1}{2}$, and up when coming in from the lower limit, 0.

In equation (8*a*) the plus sign of the buoyancy force applies for net upflow, R near 0, and the minus sign applies for net downflow, R near $\frac{1}{2}$. Clearly, sufficiently deep penetration into the region of 0 to $\frac{1}{2}$, from either side, would result in convective inversion of the whole flow. It would be inversion from downflow to upflow, coming in from $\frac{1}{2}$, and the reverse coming in from zero. One measure of the tendency toward convective inversion would be the integral across the thermal diffusion region of F, or of W, as I_w in (9). This integral will be seen to approach zero from negative values for $R < \frac{1}{2}$ and from positive ones for $R > 0$.

The basic transport quantities in terms of similarity variables are:

$$u(x,y) = \nu cbf'(\eta) = \nu \frac{G^2}{4x} f'(\eta), \tag{11}$$

$$-v(x,y) = \nu(c_x f + cf' y b_x) = \frac{\nu G}{4x}(3f - \eta f'), \tag{12}$$

$$\tau(x) = \frac{\mu \nu G^3}{16x^2} f''(0), \tag{13}$$

$$Nu_x = h_x x/k = [-\phi'(0)/\sqrt{2}]\, Gr_x^{\frac{1}{2}}, \tag{14}$$

$$\delta(x) = 4x\eta_\delta / G, \tag{15}$$

$$M_x = \int_0^\infty \rho u^2 dy = \rho \nu^2 c^2 b \int_0^\infty (f')^2 d\eta = \rho \nu^2 c^2 b I_m, \tag{16}$$

$$\dot{m} = \int_0^\infty \rho u\, dy = \nu \rho c f(\infty), \tag{17}$$

where $\tau(x)$ is the local surface shear stress, Nu_x is the local Nusselt number, $\delta(x)$ is the local boundary region thickness, M_x is the local boundary region convection of momentum and $\dot{m}$ is the mass flow both per unit width of surface, all at downstream location x. All of these quantities will be seen to behave much as when a linear temperature approximation of ρ is used, except as modified by the effect of changing R.

Equations (8*a*) and (8*b*) were solved subject to boundary conditions (8*c*) using two different numerical techniques. The first, used over the two ranges $0 \leqslant R \leqslant 0{\cdot}15$ and $0{\cdot}29 \leqslant R \leqslant 0{\cdot}50$, was a predictor–corrector shooting method. This scheme included automatic local sub-division of step size to maintain accuracy, while integrating from $\eta = 0$ to $\eta = \eta_{\text{edge}}$. Initially unknown values of $\phi'(0)$ and $f''(0)$ were guessed and subsequently corrected to satisfy the far boundary conditions. By perturbing the step size, $\Delta\eta$, and the accuracy criterion, it was determined that $\Delta\eta = 0{\cdot}05$ and a predictor–corrector accuracy criterion of 10^{-10} were sufficient to obtain values $f''(0)$, $\phi'(0)$, I_w and $f(\infty)$ unchanging to five digits. The value of η_{edge} was increased to as large as 60 in some cases to maintain this level of convergence. With this numerical method it was determined that flow reversal near the surface first occurred for R near $0{\cdot}32$. However, it was not possible to determine values of R for which outside flow reversal occurred. For $R = 0{\cdot}15$ outside flow reversal was not found and the numerical scheme would not converge for $0{\cdot}15 < R < 0{\cdot}29$.

To overcome this difficulty, a second numerical technique was used. The asymptotic solutions of equations (8*a*) and (8*b*) for ϕ, f and f' as $\eta \to \infty$ can be shown to be

$$\begin{cases} f \to A - Ce^{-3A\eta} \mp \dfrac{BRq|R|^{q-2}}{27(Pr)^2A^3(Pr-1)} e^{-3PrA\eta}, & (18a) \\ f' \to 3ACe^{-3A\eta} \pm \dfrac{BRq|R|^{q-2}}{9PrA^2(Pr-1)} e^{-3PrA\eta}, & (18b) \\ \phi \to Be^{-3PrA\eta}, & (18c) \end{cases}$$

where A, B and C are constants to be determined. Where two signs appear in (18*a*) and (18*b*), the upper sign applies for upflow and the lower sign for downflow. The asymptotic expressions in (18) are taken as exact at some sufficiently large value of $\eta = \eta_{\text{edge}}$. The constants A, B and C are guessed and the expressions in (18) are used to calculate starting values of f, ϕ and their derivatives. A predictor–corrector routine is then used with a fixed step size to integrate equations (8*a*) and (8*b*) from η_{edge} to 0. A, B and C are corrected such that the boundary conditions at $\eta = 0$ are met to within a prescribed accuracy, ϵ. By varying the step size, $\Delta\eta$, the accuracy criterion, ϵ, and η_{edge}, it was determined that $\Delta\eta = -0{\cdot}05$, $\epsilon = 10^{-10}$ and $\eta_{\text{edge}} = 20$ were adequate to obtain values of $f''(0)$, $\phi'(0)$, I_w and $f(\infty)$ unchanging to five digits.

From (18*a*) it can be seen that $A = f(\infty)$. From (18*b*) and (18*c*), if $A > 0$, then as $\eta \to \infty, f' \to 0$ and $\phi \to 0$, but if $A < 0$, then as $\eta \to \infty, f' \to \infty$ and $\phi \to \infty$. $A = f(\infty) > 0$ is therefore a necessary condition for the solution of equations (8*a*) and (8*b*) to meet the boundary conditions for f' and ϕ as $\eta \to \infty$. Accordingly, the co-ordinate system for each of the two flow regimes is oriented as in figure 1, so that the net mass flow, $f(\infty)$, is positive.

This second numerical method permitted determination of the conditions for which local flow reversal occurs at the outer edge of the flow region. Outside flow reversal occurs when the net mass flow is upward. Therefore, the plus sign applies to the second term of equation (18*b*). Since Pr appears as a factor in the exponent of the second term of (18*b*), and Pr is about 12, the second term will be several orders of magnitude smaller than the first term. Therefore, f' may be negative for large η if and only if $C < 0$. Thus, the conditions for incipient outside flow reversal can be inferred by determining the conditions for which C changes sign, i.e. at $C = 0$.

Numerical results are presented well into the range of local buoyancy force reversal, coming in from both sides. Penetration was much simpler from above, $R < \frac{1}{2}$. Then the tendency to flow reversal occurs near the surface and is strongly damped by viscous forces. From the other side, $R > 0$, reversal occurs in the outer part of the thermal region where viscous forces are very small. Numerical calculations in this range were found to be much more sensitive. However, in both ranges or R, solutions were most difficult to obtain for values of R which resulted in local flow reversal.

3. Results

The parameters of the calculations are $q(s_\infty, p)$, Pr and $R(s_\infty, p, t_0, t_\infty)$. The value of $q(s_\infty, p)$ was taken as each of its two extreme values over the range of applicability of equation (1). They are $q(0, 1) = 1{\cdot}894816$ and $q(0, 1000) = 1{\cdot}582950$. For pure water at 1000 bars, t_m is about $-17{\cdot}6\,^\circ\text{C}$ and the equilibrium melting point of ice is about

q	Pr	R	$f''(0)$	$-\phi'(0)$	$f(\infty)$	I_w	I_m
1·894816	8·6	0·0	0·34071	0·96209	0·20054	0·39088	0·01003
		0·10	0·26769	0·84458	0·15425	0·29418	0·00530
		0·14	0·23738	0·77227	0·10827	0·25217	0·00296
	11·6	0·0	0·31843	1·04697	0·18506	0·35867	0·00805
		0·05	0·28475	0·99001	0·16791	0·31587	0·00622
		0·10	0·24948	0·91836	0·14304	0·27049	0·00420
		0·14	0·22077	0·83992	0·10356	0·23229	0·00230
		0·15	0·21393	0·81084	0·07398	0·22244	0·00170
		0·15171	0·21293	0·80241	0·05346	0·22075	0·00156
		0·15172	0·21292	0·80232	0·05305	0·22074	0·00156
		0·15176	0·21291	0·80187	0·05102	0·22070	0·00156
	12·0	0·15199	0·21098	0·80904	0·05225	0·21847	0·00150
		0·15200	0·21097	0·80894	0·05181	0·21846	0·00150
	13·6	0·0	0·30709	1·09447	0·17740	0·34287	0·00716
		0·10	0·24025	0·95961	0·13739	0·25884	0·00372
		0·15	0·20570	0·84809	0·07596	0·21314	0·00149
1·582950	11·6	0·0	0·34221	1·09707	0·19927	0·39167	0·00989
		0·10	0·26642	0·94827	0·14185	0·28834	0·00438
		0·13	0·24234	0·87657	0·09471	0·25438	0·00241

TABLE 1. Transport parameters for net upward flow adjacent to a vertical isothermal surface for various q, Pr and R.

$-9{\cdot}1$ °C. Therefore, in thermodynamic equilibrium, temperature conditions do not arise for which R is between 0 and $\frac{1}{2}$. However, in freezing, non-equilibrium surface temperature depressions may be great enough to result in values of R between 0 and $\frac{1}{2}$. Such conditions have been observed at lower pressures. For example, Caldwell (1980) has reported cooling pure water to its extremum temperature, $t_m(0, p)$, at pressures as high as 380 bars. This amounts to subcooling of about 2 °C below the equilibrium melting temperature of pure water at 380 bars. Nevertheless, these conditions are not frequently encountered. The results are presented rather to assess the effect of different values of q on transport and to allow interpolation of the results for values of q at other salinities and pressures.

The chosen values of Pr = 8·6, 11·6 and 13·6 apply for pure water at 1 atm at temperature levels of about 13, 4 and 0 °C. The variation of Pr is mainly due to viscosity. Mollendorf, Kukulka & Gebhart (1980) summarize data showing that Pr is not sharply dependent on either s or p, to 40‰ and to 1000 bars.

Calculations were carried out for $q(0, 1)$ for Pr = 8·6, 11·6 and 13·6 to assess the Prandtl number effect, then for $q(0, 1000)$ and Pr = 11·6 to determine the effect of q. For each of these four sets of q and Pr, calculations were done for various values of R, increasingly inward from both boundaries of the region $0 < R < \frac{1}{2}$. For Pr = 11·6 and $q(0, 1)$, solutions were obtained for $0 \leqslant R \leqslant 0{\cdot}15176$ and for $0{\cdot}292 \leqslant R \leqslant \frac{1}{2}$. Calculated transport parameters for net upward flow and net downward flow are summarized separately in tables 1 and 2, respectively.

The numerical results, using the asymptotic method, for values of R in the lower range, are given in table 3. The computed values of A, B and C near the condition of outside flow reversal are shown for $q(0, 1)$ for Pr = 11·6 and 12·0. The radius of convergence of the (A, B, C) vector is very small near R = 0·15, which necessitated very accurate initial guesses of A, B and C to obtain convergence. As seen in table 3, for

q	Pr	R	$f''(0)$	$-\phi'(0)$	$f(\infty)$	I_w	I_m
1·894816	8·6	0·30	−0·05763	0·54803	0·19232	0·01831	0·00786
		0·32	−0·01341	0·64803	0·19867	−0·02928	0·00854
		0·40	0·09039	0·82219	0·21904	−0·14817	0·01156
		0·50	0·18545	0·94073	0·23784	−0·26036	0·01498
	11·6	0·292	−0·07983	0·51253	0·17506	0·04817	0·00633
		0·30	−0·04692	0·61582	0·17727	0·01503	0·00638
		0·32	−0·00825	0·71439	0·18302	−0·02652	0·00695
		0·40	0·08779	0·89922	0·20172	−0·13476	0·00939
		0·50	0·17665	1·02713	0·21903	−0·23743	0·01216
	13·6	0·30	−0·04228	0·65248	0·16987	0·01375	0·00571
		0·32	−0·00596	0·75137	0·17533	−0·02518	0·00623
		0·40	0·08623	0·94235	0·19321	−0·12827	0·00841
		0·50	0·17193	1·07553	0·20979	−0·22629	0·01087
1·582950	11·6	0·29	−0·04807	0·65301	0·18784	0·01008	0·00760
		0·30	−0·02516	0·70979	0·19052	−0·01423	0·00788
		0·32	0·00936	0·78467	0·19552	−0·05186	0·00850
		0·40	0·10644	0·94954	0·21135	−0·16073	0·01086
		0·50	0·19671	1·06494	0·22534	−0·26323	0·01330

TABLE 2. Transport parameters for net downward flow adjacent to a vertical isothermal surface for various q, Pr and R.

q	Pr	R	A	B	C
1·894816	11·6	0·10	0·14304	44768·0	0·15725
		0·15	0·07398	146·17	0·031366
		0·15171	0·05346	2·5165	0·00029226
		0·15172	0·05305	2·2689	−0·00026827
		0·15176	0·05102	1·3371	−0·0030029
	12·0	0·15199	0·05225	2·6170	0·00047711
		0·15200	0·05181	2·3316	−0·00011390

TABLE 3. Constants for the asymptotic solution for large η for the indicated values of q, Pr and R.

$Pr = 11{\cdot}6$, C first becomes negative for $R = 0{\cdot}15172$. The computed velocity profile reversed from positive to negative at approximately $\eta = 5{\cdot}5$. The value of R for which outside flow reversal first occurs was also determined for $q(0, 1)$ and $Pr = 12{\cdot}0$, since these are exactly the values of q and film Prandtl number for ice melting in fresh water for $R = 0{\cdot}152$, corresponding to $t_\infty = 4{\cdot}75\,^\circ\mathrm{C}$. The results therefore indicate that for melting of ice in pure water, incipient outside flow reversal occurs for $R = 0{\cdot}152$ or $t_\infty = 4{\cdot}75\,^\circ\mathrm{C}$. Further, comparison with the results for $Pr = 11{\cdot}6$ indicates that increasing Pr slightly increases the value of R for which local incipient outside flow reversal occurs.

In the higher range of R, incipient inside flow reversal may be detected in table 2 as the value of R for which $f''(0)$ first becomes negative. This occurs at about $R = 0{\cdot}32$. The plot of $f''(0)$ versus R in figure 3 indicates that the precise value depends on both q and Pr. For ice melting in fresh water, $q = q(0, 1)$ and the value of Pr at the film temperature for $R = 0{\cdot}326$ is equal to 11·7. For these conditions, incipient inside flow reversal occurs for $R = 0{\cdot}326$ corresponding to $t_\infty = 5{\cdot}98\,^\circ\mathrm{C}$. Of course, the boundary-layer

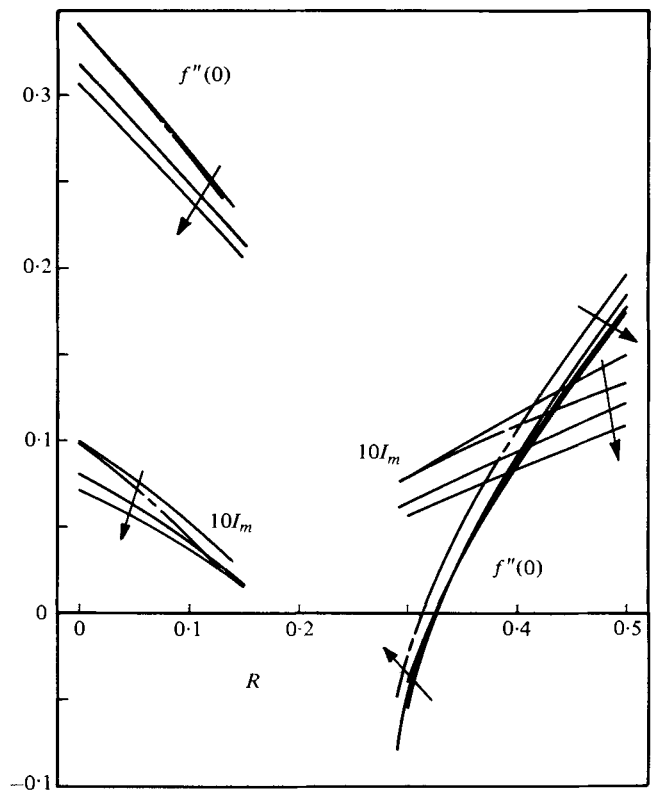

FIGURE 3. The local shear stress parameter, $f''(0)$, and I_m variation with R. The broken curves are $q = q(0, 1000)$ and $Pr = 11{\cdot}6$. For the solid curves (——), $q = q(0, 1)$ and the arrows indicate increasing Pr for $Pr = 8{\cdot}6$, $11{\cdot}6$, and $13{\cdot}6$.

assumptions strictly become inapplicable for bi-directional flow. Hence, the conditions for incipient local flow reversal are of considerable importance since they define the probable range of validity of the present analysis.

The tangential velocity component distributions, f', are shown in figure 4, for $q(0, 1)$ and $Pr = 11{\cdot}6$, for both ranges of R. Note that $-f'$ is plotted for the downward flows. Thereby the relative directions of the tangential velocity in each flow regime are properly oriented. Weakening upflow and downflow are seen, away from $R = 0$ and $\frac{1}{2}$, respectively, as local buoyancy-force reversals increase. The distributions of the local buoyancy force, $W(\eta)$, are plotted in figure 5.

Consider first the simpler circumstance, the upper range of R with inside reversal. Local upflow reversals are seen near the surface in figure 4 for the general downflows which accompany both $R = 0{\cdot}30$ and $R = 0{\cdot}292$. The relation of $W(\eta)$ to this effect is clear in figure 5. There W is seen to be negative over a large part of the boundary region. Even though it is large and positive over an appreciable region near the surface, only a small local flow reversal arises. This is due to the opposition of the large downward viscous forces in the fluid near the surface to the upward buoyancy there. For $R = 0{\cdot}32$ and $0{\cdot}40$ appreciable local flow reversal does not occur, in spite of large regions of positive W.

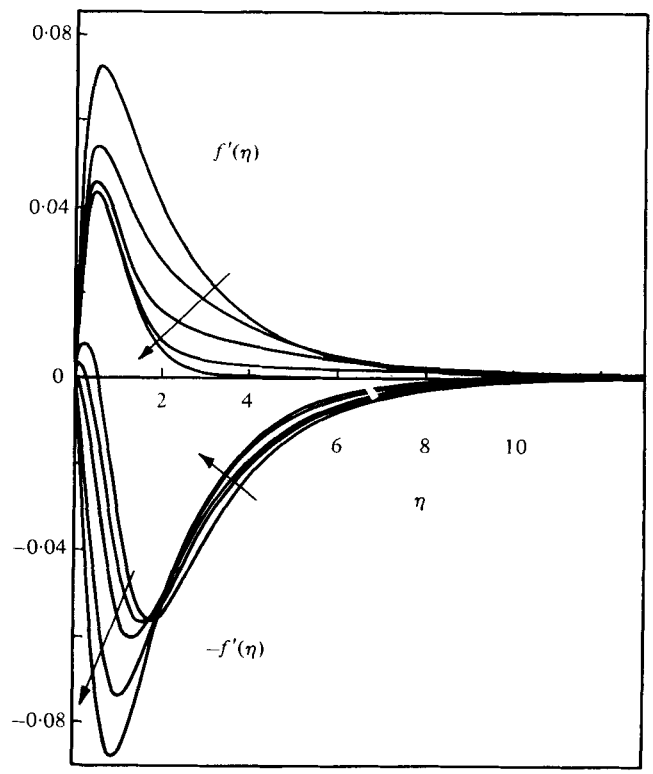

FIGURE 4. Distributions across the flow layer of the tangential component of velocity, f' for upward flow and $-f'$ for downward flow, for $q(0, 1)$ and $Pr = 11{\cdot}6$. For upflow the arrow indicates increasing R for $R = 0$, 0·10, 0·14, 0·15 and 0·15172. For downflow the arrows indicate increasing R for $R = 0{\cdot}292$, 0·30, 0·32, 0·40 and 0·50.

For R increasing from zero, there is a range of R for which there is no local flow reversal, even though W changes sign across the thermal region. These small buoyancy-force reversals lie around $\eta = 1{\cdot}5$, well inside the flow region. A large viscous force there, together with high momentum, is able to overcome this effect.

Another principal effect on the velocity field is seen in figure 6, where $3f - \eta f'$ is plotted across the boundary region. This quantity is proportional to $v(x, y)$, the component of velocity normal to the surface, see (12), where $3f(\infty)$ becomes the entrainment velocity generated by the flow in the ambient medium. The flow decreases as buoyancy-force reversal increases and a change in direction occurs near the surface for $R = 0{\cdot}32$ and $R = 0{\cdot}292$. Note that, except for this circumstance, the flow is toward the surface, with positive entrainment. A similar reversal in $v(x, y)$ was observed by Mollendorf, Johnson & Gebhart (1980) for the axisymmetric and plane wall plumes in ambient water at t_m. The entrainment parameter, $f(\infty)$, is also plotted versus R in figure 7.

However, the effects of W reversal on other transport quantities are very large, especially for an inside reversal of W, where results were obtained for the wider range of R. The local surface shear stress parameter $f''(0)$, plotted in figure 3, shows a dramatic decrease toward zero as convective inversion is approached from the upper range. It

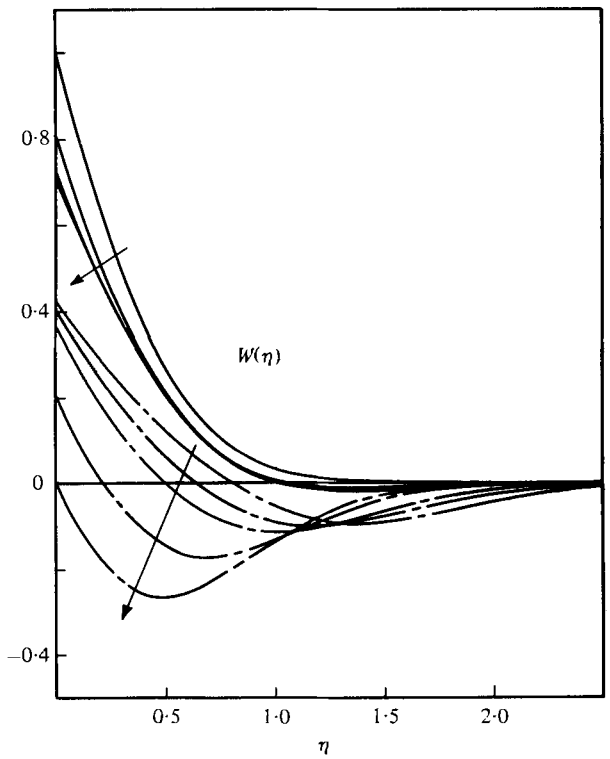

FIGURE 5. Distributions of the local buoyancy force, W, across the thermal diffusion region for $q(0, 1)$ and $Pr = 11{\cdot}6$. For net upward flow (——) the arrow indicates increasing R for $R = 0$, 0·10, 0·14, 0·151 72. For net downward flow (— — —) the arrow indicates increasing R for $R = 0{\cdot}292$, 0·30, 0·32, 0·40, 0·50.

has actually changed direction for $R = 0{\cdot}32$ and $R = 0{\cdot}292$, even though the net flow is still strongly down. Such a reversal of surface shear stress before inversion does not occur as the inversion condition is approached in the lower range. There, local flow reversal occurs in the outer part of the boundary region.

Also of interest in figure 3 is the variation with R of I_m, the local momentum flux. By integrating equation (8a) from $\eta = 0$ to $\eta = \infty$ and applying the boundary conditions in (8c), it can be shown that

$$I_m = \int_0^\infty (f')^2 d\eta = \tfrac{1}{5}[\pm I_w - f''(0)], \tag{19}$$

where for I_w, the plus sign applies for net upflow and the minus sign applies for net downflow. Note that I_m is proportional to the tangential momentum convected downstream at location z and is a measure of the vigour of the flow. Equation (19) shows that the rate at which momentum is imparted to the flow is proportional to the difference between the integral of the buoyancy force and the shear stress at the surface. Further, $I_m > 0$, necessarily. Then if $\pm I_w < 0$, clearly $f''(0) < 0$. This occurs for R near 0·30. Figure 6 indicates that for R near 0·15, I_m decreases sharply with increasing R. This suggests an approach to convective inversion. However, for R near 0·30, the flow retains considerable vigour despite the net reversal in buoyancy force, I_w, see table 2.

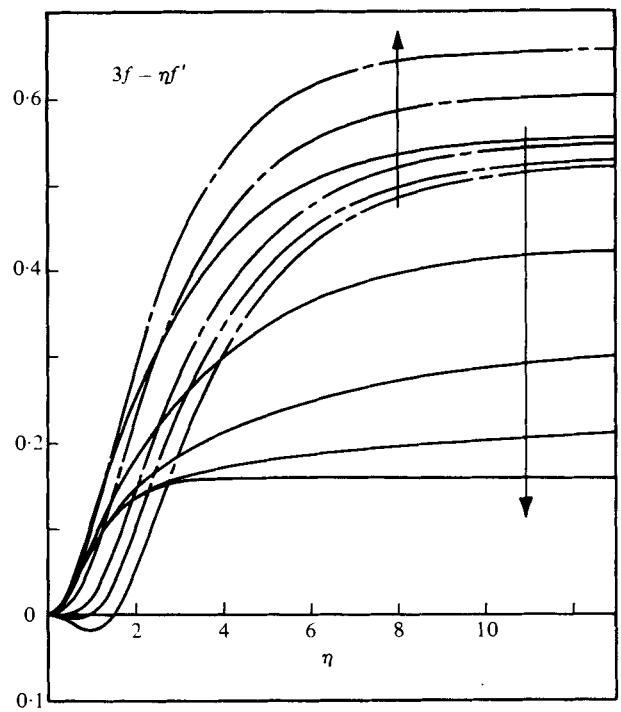

FIGURE 6. Distributions of the normal and entraining velocity component for $q(0, 1)$ and Pr = 11·6. For net upward flow (——) the arrow indicates increasing R for R = 0, 0·10, 0·14, 0·15 and 0·151 72. For net downward flow (— — —) the arrow indicates increasing R for R = 0·292, 0·30, 0·32, 0·40 and 0·50.

These very complicated implications of convective inversion are more clearly seen in figure 7 where I_w and $f(\infty)$ are plotted as a function of R for each of the four q and Pr conditions considered. Clearly, I_w goes sharply toward zero on both sides as convective inversion is approached. However, a most surprising result is seen at R = 0·30. For example, for $q(0, 1)$ at Pr = 11·6, I_w has become positive even though the net flow is still strongly downward (recall figure 4). Thus, the integrated upward buoyancy force near the surface, although larger, is damped by viscous forces and the smaller integral of downward buoyancy force in the outer region still determines the net flow direction.

Thus, it is not possible to directly surmise from these results the exact condition of convective inversion. Because of the boundary-layer approximations employed here, there is large uncertainty associated with extrapolation to conditions for which bi-directional flow occurs. However, if small local flow reversals are tolerated, the results indicate that $I_w = 0$ is, in fact, not a criterion for convective inversion. As inversion is approached from R = 0·50, I_w must actually become substantially positive before inversion will occur because of the shear force it must overcome near the surface.

The ice-melting experiments of Bendell & Gebhart (1976) indicated that net flow was up for t_∞ = 5·5 °C and down for 5·6 °C. The condition for convective inversion was therefore t_∞ = 5·55 °C or R_c = 0·28. In figure 7, R_i values, where $I_w = 0$, are marked on the curves of I_w at 0·307 for $q(0, 1)$ for Pr = 11·6, The results of Bendell & Gebhart (1976) are therefore consistent with the present results which show that $R_c < R_i =$

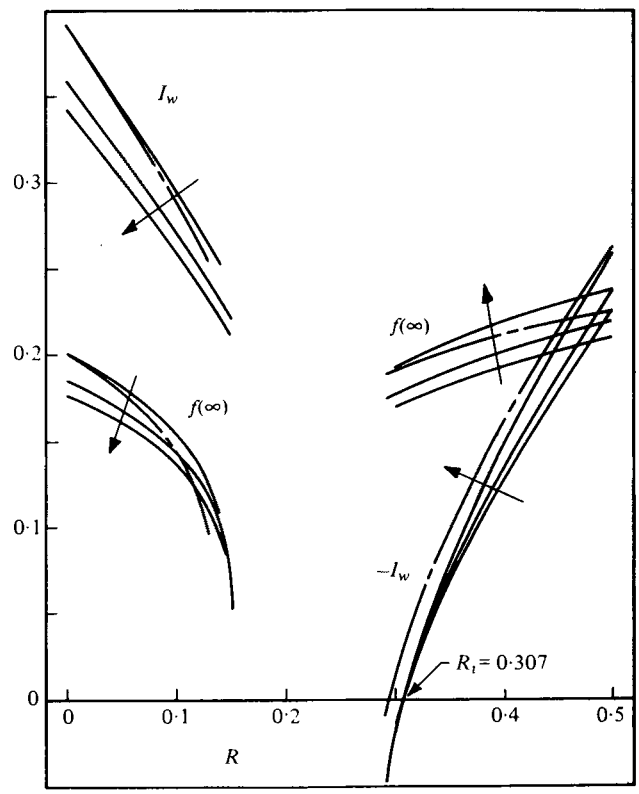

FIGURE 7. The mass flow, $f(\infty)$, and I_w variations with R. The broken curves (– – –) are $q = q(0, 1000)$ and $Pr = 11{\cdot}6$. For the solid curves (——), $q = q(0, 1)$ and the arrows indicate increasing Pr for $Pr = 8{\cdot}6$, $11{\cdot}6$ and $13{\cdot}6$.

0·307. However, a completely different result is suggested by the calculations in the lower range. In figure 7 there is a very rapid decrease in mass flow, $f(\infty)$, as R increases near $R = 0{\cdot}15$. If we may extrapolate these results, this suggests that the net mass flow becomes negative, i.e. convective inversion occurs near $R = 0{\cdot}16$.

Convergent numerical solutions could not be obtained for $0{\cdot}15176 < R < 0{\cdot}292$. Hence it is not possible to make a definitive statement about the behaviour of the flow for values of R in this range. However, the results obtained for $R = 0{\cdot}15176$ and $R = 0{\cdot}292$ suggest that the flow may be bi-directional for $0{\cdot}15176 < R < 0{\cdot}292$.

Buoyancy force reversals also cause large and important effects on thermal transport, as seen in figures 8 and 9. The temperature distributions, $\phi(\eta)$ in 8, seem relatively little affected in form. However, their slope at $\eta = 0$, $-\phi'(0)$, determines the local heat transfer rate. Figure 9 indicates large decreases in heat transfer as convective inversion is approached. The data of Bendell & Gebhart (1976) and of Johnson & Mollendorf (1980) are plotted for comparison. Interface motion, or equivalently, interface blowing, known to be present in ice-melting experiments at low temperatures, has only a small effect on transport. Of the conditions considered here, the greatest interface velocity occurs at $R = 0{\cdot}5$, for which the heat flux to the surface is the greatest. To assess this effect, the present analysis was modified to include interface blowing and the solution

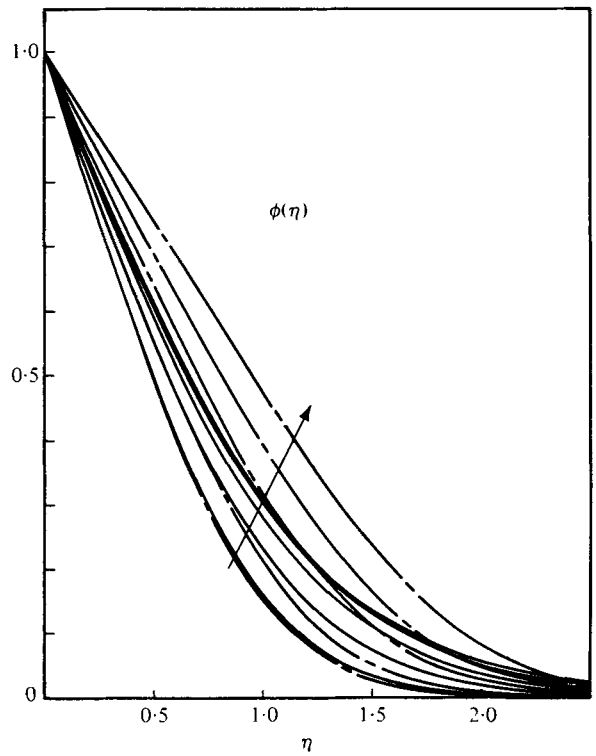

FIGURE 8. Distributions of the temperature variation, $\phi(\eta)$, across the thermal diffusion region for $q = q(0, 1)$ and $Pr = 11{\cdot}6$. For net upward flow (——), the arrow indicates increasing R for $R = 0, 0{\cdot}10, 0{\cdot}14, 0{\cdot}15, 0{\cdot}151\,72$. For net downward flow (— — —), the arrow indicates decreasing R for $R = 0{\cdot}50, 0{\cdot}40, 0{\cdot}32, 0{\cdot}30, 0{\cdot}292$.

was computed for $R = 0{\cdot}50$ and $Pr = 11{\cdot}6$. For these conditions, the surface heat transfer decreased by 5 %. At lower values of R the blowing velocity is smaller, with a smaller effect on transport. Hence for ice-melting in pure water with $0 \leqslant R \leqslant 0{\cdot}5$, the computed results without interface blowing should be accurate within 5 %. The comparison of these results with the experimental ice-melting data is therefore appropriate.

The value of $-\phi'(0)$ is related to the experimental average Nusselt number as

$$-\phi'(0) = \frac{3\sqrt{2}}{4} Nu_L/(Gr_L)^{\frac{1}{4}}. \tag{20}$$

The values of Nu_L from Bendell & Gebhart (1976) have been multiplied by $\rho_{\text{ice}}/\rho_\infty$ to correct an error in the computation of Nu_L from the measured melting rates. Note that the data levels of Pr lie in the range from 11·3 to 12·0. The r.m.s. difference for the ten data points shown is only 9·2 %. This is certainly within the expected accuracy of the data. However, both sets of data are systematically slightly lower than the computed results. Since our calculations do not include the effects of interface blowing, the results may be as much as 5 % higher than the actual surface heat transfer rate for ice melting in pure water. We therefore conclude that the experimental data is systematically lower than the computed results primarily as a consequence of interface blowing effects.

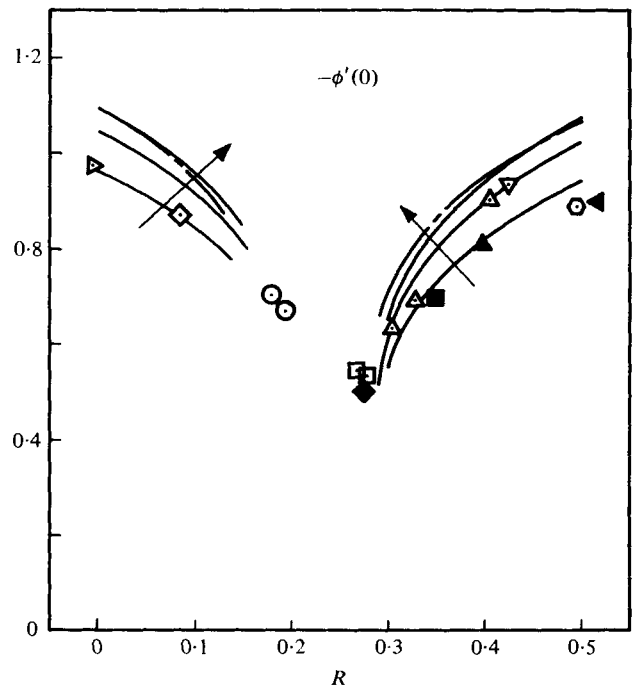

FIGURE 9. The variation of the calculated heat transfer parameter, $\phi'(0)$, with R. The broken curves (– – –) are $q = q(0, 1000)$ and $Pr = 11{\cdot}6$. For the solid curves (——), $q = q(0, 1)$ and the arrows indicate increasing Pr for $Pr = 8{\cdot}6$, $11{\cdot}6$ and $13{\cdot}6$. Also shown are the data of Bendell & Gebhart (1976) and Johnson & Mollendorf (1980), determined for ice melting in pure water. Bendell & Gebhart's (1976) film Prandtl numbers are: ⊙, 11·3; ▽, 11·5; △, 11·7; ⊡, 11·8; ○, 11·9; ◇, 12·0; ▷, 12·1. Johnson & Mollendorf's (1980) film Prandtl numbers are: ◀, 11·4; ▲, 11·7; ■, 11·8; ◆, 12·0.

Nevertheless, the present calculations are in good agreement with the data in both the upflow and downflow regions.

4. Conclusions

Computed results for laminar natural-convection flow adjacent to a vertical isothermal surface in cold water have been presented for a range of conditions for which the buoyancy force is bi-directional across the thermal layer. These results apply to a heated or cooled vertical isothermal surface in pure or saline water when $0 \leqslant R \leqslant 0{\cdot}5$. For pure water at 1 bar, incipient local flow reversal occurs near the outside of the flow region for $R = 0{\cdot}152$. Incipient local flow reversal occurs near the surface for $R = 0{\cdot}326$. This suggests that for $0{\cdot}152 < R < 0{\cdot}326$ the flow is bi-directional near $R = 0{\cdot}152$ and $0{\cdot}326$ where the local flow reversals are small. However, in the centre of the interval $0{\cdot}152 < R < 0{\cdot}326$, the flow may be bi-directional or may have an entirely different character. It may, for example, be steady two-dimensional flow with recirculation or it may take a form which is time dependent.

Convective inversion does not occur for R_i, i.e. when $I_w = 0$, but rather for some $R_c < R_i$ for which $I_w > 0$. This is due to the viscous forces near the surface which

sharply damp the effect of the buoyancy force reversal there. Here R_i was found to be 0·307 for $Pr = 11{\cdot}6$ and $q(0, 1)$. The computed results imply that for fresh water at 1 bar, convective inversion occurs at some value of $R = R_c$ between 0·152 and 0·292. The limits on R_c and the conditions for incipient local flow reversal appear to be only weakly dependent on Pr and $q(s_\infty, p)$.

Surface heat transfer decreases rapidly as convective inversion is approached both from $R = 0$ and $R = \frac{1}{2}$. The lowest surface heat transfer rate is only 50 % of that for both $R = 0$ and $R = \frac{1}{2}$, where the buoyancy force acts entirely in one direction.

For ice melting in pure water at 1 bar the range $0 \leqslant R \leqslant 0{\cdot}5$ corresponds to ambient water temperatures between 4 and 8 °C. At these low ambient temperatures the ice melt rate is slow and consequently the interface blowing velocity is small. Sample calculations including interface blowing indicate that the effect of interface blowing on transport is small for these conditions. Interface blowing reduces heat transfer by less than 5 %. Although they do not include interface blowing, the computed results may therefore be applied to a vertical ice surface melting in pure water with only a very small loss in accuracy.

The calculated surface heat transfer is in good agreement with that inferred from ice melting rates measured in the experiments of Bendell & Gebhart (1976) and Johnson & Mollendorf (1980), in both flow regimes. The calculated values of surface heat transfer imply, for example, that for a vertical ice surface 30 cm high melting in pure water at 1 bar, the melting rate decreases from 0·52 cm/h at $t_\infty = 4{\cdot}0$ °C to 0·43 cm/h for $t_\infty = 5{\cdot}7$ °C. Although $t_\infty - t_0$ has been increased by 40 %, the melt rate decreases by 17 %. In addition, the computed results predict that for ice melting in pure water at 1 bar, the flow is bi-directional for t_∞ between 4·75 °C and 5·98 °C and that convective inversion occurs at some ambient temperature between 4·75 °C and 5·81 °C. It was not possible to further refine this interval. However, this agrees with the experiments of Bendell & Gebhart (1976) which indicate that convective inversion occurs for t_∞ between 5·5 and 5·6 °C.

It may also be possible to apply the computed results to freezing of a vertical ice surface in pure water, provided the freezing rate is sufficiently slow that interface motion effects are small. For freezing, the interface motion is treated as interface suction. Since blowing reduces surface heat transfer, it is expected that suction increases it. It is likely, therefore, that the results computed with no interface suction will predict surface heat transfer rates that are slightly low. However, for low freezing rates the loss in accuracy should be small.

These flows are found to be relatively very weak; particularly so for conditions near convective inversion. However, the resulting mass and thermal transport is highly sensitive to the exact values of the imposed temperature conditions, which suggests the possibility of early downstream laminar instability.

The first author wishes to acknowledge graduate fellowship support from the Woodburn Foundation. The authors also wish to acknowledge support for this study by the National Science Foundation under research grants ENG77-21641 (V. P. Carey and B. Gebhart) and ENG76-16936, ENG77-27945 (J. C. Mollendorf).

REFERENCES

BENDELL, M. S. & GEBHART, B. 1976 Heat transfer and ice-melting in ambient water near its density extremum. *Int. J. Heat & Mass Transfer* **19**, 1081–1087.

CALDWELL, D. R. 1980 The maximum density points of saline water. Submitted to *Deep-Sea Res.*

CHEN, C. T. & MILLERO, F. J. 1976 The specific volume of sea water at high pressures. *Deep Sea Res.* **23**, 595–612.

FINE, R. A. & MILLERO, F. J. 1973 Compressibility of water as a function of temperature and pressure. *J. Chem. Phys.* **59**, 5529–5536.

GEBHART, B., CAREY, V. P. & MOLLENDORF, J. C. 1980 Buoyancy induced flows due to energy sources in cold quiescent pure and saline water. *Chem. Engng Trans.* (to appear).

GEBHART, B. & MOLLENDORF, J. C. 1977 A new density relation for pure and saline water. *Deep Sea Res.* **24**, 813–848.

GEBHART, B. & MOLLENDORF, J. C. 1978 Buoyancy-induced flows in water under conditions in which density extrema may arise. *J. Fluid Mech.* **89**, 673–707.

JOHNSON, R. S. & MOLLENDORF, J. C. 1980 Transport from a vertical pure water ice surface melting in saline water. In preparation.

MOLLENDORF, J. C., JOHNSON, R. S. & GEBHART, B. 1980 Several constant buoyancy plume flows in cold pure and saline water. Submitted to *J. Fluid Mech.*

MOLLENDORF, J. C., KUKULKA, D. & GEBHART, B. 1980 Transport properties of seawater. In preparation.

QURESHI, Z. H. & GEBHART, B. 1978 Vertical natural convection with a uniform flux condition in pure and saline water at the density extremum. *Proc. 6th Int. Heat Transfer Conf., Toronto.*